JOURNAL OF GEOPHYSICAL RESEARCH, VOL. 98, NO. A5, PAGES 7609–7620, MAY 1, 1993

Testing the Isotropic Boundary Algorithm Method to Evaluate the Magnetic Field Configuration in the Tail

V. A. SERGEEV

Institute of Physics, University of St. Petersburg, Russia

M. MALKOV

Polar Geophysical Institute, Apatity, Russia

K. MURSULA

Department of Physics, University of Oulu, Oulu, Finland

Simultaneous measurements of the low-altitude energetic particle flux by NOAA spacecraft and the geostationary magnetic field by GOES 2 spacecraft are used to test the recently proposed isotropic boundary algorithm (IBA) method to evaluate the instantaneous magnetospheric configuration. According to the IBA method, the equatorward boundary of the isotropic proton precipitation, in brief the isotropic boundary (IB), corresponds to the boundary separating adiabatic and chaotic regimes of particle motion in the tail current sheet and is controlled by the properties of the equatorial magnetic field. In this study we confirm some of the fundamental features of the IBA method. First, we show that the low-altitude IB position of 30– to 300–keV protons is strongly controlled by the equatorial magnetic field in the tail. (The corresponding correlation coefficient exceeds 0.9.) Second, the MLT dependence of the nightside IB latitude is in good agreement with that computed using magnetospheric models. Third, the observed magnetic field and the field predicted by the IBA method using the measured IB position have similar values and are well correlated with a correlation coefficient of at least 0.84 for the main components and a standard deviation of only about 10 % of the dynamic range of these components. This shows that the threshold condition separating the two particle motion regimes is fulfilled in the proximity of the IB field line. We argue that the remaining inconsistencies between the calculated and observed magnetic fields are mainly due to the fact that the available magnetospheric models seem to underestimate the amount of tailward stretching of both the tail field lines during active conditions as well as field lines starting from the dayside. In view of its good capabilities to remotely determine the instantaneous magnetic field, we expect that the IBA method will find wide applications in the mapping of magnetic field lines and in testing of existing and new magnetospheric models.

1. INTRODUCTION

The magnetic field in the tail is strongly influenced by changing solar wind conditions as well as internal magnetospheric processes like substorms and is very variable on a typical time scale from a few minutes to tens of minutes. Accordingly, for many applications and studies, it is important to know the instantaneous magnetospheric configuration. This is true, for example, when trying to use the extensive information available from low-altitude and ground-based observations to study the dynamic processes in the magnetotail plasma sheet, as well as when comparing low-altitude observations to those made in the magnetosphere. An illustration of problems resulting from the ignorance of the instantaneous magnetic field configuration is the great auroral mapping controversy in identifying the magnetospheric source regions of auroral arcs and the different types of auroral particle precipitation [see *Siscoe*, 1991]. The need for three-dimensional studies of magnetospheric processes is a great challenge to the forthcoming space projects (e.g., ISTP, Interball, and Cluster) and the success of these studies is highly dependent on solving the mapping problem.

An important fact when considering mapping is that the equatorial plasma sheet and ionospheric regions are decoupled in several ways. First, direct comparison of the plasma properties in the two domains can hardly yield definite results. The spectral characteristics of plasmasheet particles measured at low altitudes are contaminated by the complicated acceleration mechanisms which operate in the high-altitude ionosphere. Second, during the substorm expansion phase the two domains are electrically decoupled since the electric field is not mapped because of the strong inductive electric fields present in the magnetosphere. Therefore mapping along the magnetic field lines is probably the most direct and reliable way to perform the mapping between the two regions.

So far, two basically different approaches to direct field line mapping were discussed in the literature: global and local models. The recent development of empirical global magnetospheric models (see *Tsyganenko*, [1990] for a review) has lead to their extensive use in direct field line mapping. However, there are two serious problems with these models. First of all, these models only represent an averaged field configuration and their applicability to any specific situation is therefore always questionable. Extreme

Paper number 92JA02587.
0148-0227/93/92JA-02587$05.00

situations like a narrow auroral oval at the end of the growth phase or a very expanded oval at the end of the expansion phase differ by an order of magnitude in the amount of magnetic flux enclosed by the oval. Obviously, they cannot be represented by the same averaged model configuration. This imperfect model problem has another aspect: global models include systematic deviations in specific regions of the magnetosphere. Most models overestimate the field magnitude in the flux tubes of the cusp/cleft domain and underestimate the tailward stretching of the field lines in the near tail during active conditions [*Tsyganenko*, 1990; *Fairfield*, 1991; *Malkov and Sergeev*, 1991].

Another serious problem is the problem of choice: how to choose the model that best corresponds to the actual magnetic field configuration during the time period to be analysed. The Kp and AE indices which are used to parameterize the different variants of these models are bad indicators of the instantaneous magnetospheric configuration. This was recently demonstrated by *Malkov and Sergeev* [1991] in their study of a long steady convection interval when the Kp and AE indices were steady over many hours. The values of the H (B_z) component measured by the spacecraft at the geostationary orbit appeared to deviate by as much as 25–30 nT from the values given by models selected according to the Kp and AE indices. Also, the error in the predicted polar cusp location was as large as 4-5 deg of latitude.

Accordingly, direct field line mapping using existing global magnetospheric models is very uncertain. The main difficulty is that errors in mapping can not be controlled but can be large. The two kinds of problems discussed above represent the price we have to pay for the globality of these models. Of course, direct magnetic measurements by magnetospheric spacecraft can help in solving the problem of choice. However, single-point measurements of magnetic field cannot solve the imperfect model problem. Multipoint measurements by several spacecraft are needed for that purpose.

The other approach to direct mapping is based on a local magnetic field model constructed for a specific time interval. This approach, which requires simultaneous magnetic observations made by several spacecraft, was recently used in substorm growth phase studies by *Sergeev et al.* [1990] and *Pulkkinen et al.* [1991, 1992]. However, the applicability of local models is strictly limited to the space covered by the spacecraft constellation. Furthermore, only relatively simple and large-scale current systems can be reproduced by the data from just a few spacecraft. Therefore this approach will hardly be useful for substorm expansion phase studies because of the strong local distortions caused by the substorm current wedge and other complicated local current systems.

In addition to these direct field line mapping methods, there exists an indirect method to evaluate the magnetic field configuration and to probe magnetic field gradients via the remote sensing of the magnetic field by low-altitude spacecraft. According to this isotropic boundary algorithm (IBA) method, as first discussed by *Sergeev and Malkov* [1988], the isotropic boundary (IB) of energetic particles measured at low altitudes is interpreted as the boundary between the regions of adiabatic and stochastic particle motion in the equatorial tail current sheet. This imposes a constraint to the equatorial magnetic field on that field line where the isotropic boundary of energetic particle precipitation is observed. Using an iterative procedure, it is possible to adjust the magnetospheric model so that this constraint is fullfilled on the field line of the observed IB position. By measuring the IB positions for particles of different energies (or for different species) it is possible to evaluate the equatorial magnetic field on different field lines, allowing one to study field gradients at the equator. The IB method has several important advantages:

1. Instantaneous probing of the magnetospheric field in different activity conditions and substorm phases is possible.
2. The magnetic configuration is determined just where the different types of auroral precipitation are directly measured. This is important when solving the auroral mapping controversy and interpreting the ground-based and low-altitude measurements.
3. The indirect information obtained about magnetic field gradients allows a determination of the quality of existing magnetospheric models and will help the development of new time varying magnetospheric models in the future.

So far, the weak point of the IBA method has been that it was based on the interpretation that the isotropic particle precipitation is only due to the tail current sheet scattering (TCS) mechanism, although other mechanisms like scattering by fluctuating E-B fields (waves) are known. Although much evidence has been presented in favor of the TCS mechanism, including the direct measurements in the magnetosphere [*West et al.*, 1978] and the simple and repetitive morphological patterns of precipitation characteristics at low altitudes [*Imhof et al.*, 1977, 1979; *Lundblad et al.*, 1979; *Sergeev et al.*, 1983; *Imhof*, 1988], it is still necessary to clarify some of the key questions concerning the nature of the isotropic boundary of the energetic particle precipitation. The most important issue is to confirm directly and in a quantitative manner that the IB position is indeed controlled by the tail magnetic field and that it is really observed on those field lines where the threshold condition for the TCS mechanism is fulfilled. In order to achieve this goal it is necessary to carry out a large quantitative comparison between the particle precipitation boundaries at low altitudes and the magnetic field measured simultaneously by a magnetospheric spacecraft. Such a quantitative comparison is one aim of the present paper. We use particle measurements by the NOAA spacecraft to determine the isotropic boundaries and the magnetic measurements by the geostationary GOES 2 spacecraft to probe the tail magnetic field. We will be mainly interested in the isotropic boundaries of protons. A more detailed discussion on the electron IB properties will be published later.

The paper is organized as follows. In the following section we present the basic features of isotropic boundaries and the IBA method. We will also study the MLT dependence of the proton isotropic boundary by comparing model predictions and observations. In section 3 we evaluate the degree to which the IB position is controlled by the tail magnetic field and test the IBA algorithm on a large data set of simultaneous magnetospheric and low-altitude observations. Section 4 discusses the TCS mechanism as the dominant source of isotropic precipitation and the

capabilities of the IBA algorithm. Furthermore, we point out some inconsistencies of the present magnetospheric models that are evident on the basis of the IBA analysis. In section 5 we present our conclusions.

2. Characteristics of the Isotropic Boundary and the Isotropic Boundary Algorithm

2.1. *Isotropic Boundary as Observed at Low Altitudes*

Particle observations used here were obtained by the space environment monitor (SEM) instrument package on board the NOAA/TIROS, NOAA-6 and NOAA-7 spacecraft. These operational spacecraft fly on nearly circular Sun-synchronous polar orbits at the altitude of about 800 km. Two spacecraft are operating simultaneously in the 0900–2100 LT and 0300–1500 LT meridional planes. The medium energy proton and electron detector (MEPED) instrument included in SEM measures with the time resolution of 2 s the differential flux of protons in the energy ranges of 30–80 keV, 80–250 keV, 250–800 keV etc., as well as the integral flux of electrons with an energy in excess of 30 keV, 100 keV, and 300 keV. The geometric factor of the MEPED instrument is about 0.0095 cm^2 ster. The MEPED instrument includes a pair of detectors, one looking radially outward and the other in a perpendicular direction. At high latitudes the former measures precipitating particles in the central part of the loss cone and the latter detects locally trapped particles outside the nominal loss cone. In addition, the total energy detector (TED) instrument was used to give information about the total energy flux of precipitating auroral electrons in the energy range between 300 eV and 20 keV. The SEM instruments are described in detail by *Hill et al.* [1985].

Two representative examples characterizing the isotropic boundary of energetic particles are given in Figures 1 and 2. Figure 1 presents the particle flux variations during a southern hemisphere pass of the TIROS spacecraft (orbit 4368) on a disturbed period (AE = 700 nT; substorm recovery phase) on August 19, 1979. For comparison, Figure 2 displays the data from the same spacecraft over the same MLT sector but during a long quiet period (AE was less than 100 nT for 9 hours before and many hours after this observation; Kp was $\leq$1). Furthermore, during the latter event there were remnants of significant fluxes of solar energetic particles in the polar cap region which helped to visualize the isotropic precipitation. Outside this region the proton fluxes seem to have a smaller intensity during the quiet period. The solar particle event started in the middle of August 19, i.e., after the pass of Figure 1.

In spite of large differences in activity conditions, in the level of particle fluxes and in the latitudes of observed structures, both figures show the following morphological characteristics of energetic particle precipitation:

1. At each crossing of the auroral zone (monitored by the TED flux), there exists a sharp boundary in both proton and electron fluxes separating the poleward zone of isotropic precipitation ($J_T \sim J_P$) from the equatorial zone characterized by weak filling of loss cone ($J_T >> J_P$). This is the isotropic boundary according to our definition. However, as seen, for example, at about 19000 s UT in Figure 1, there may be some small scale structures around the IB where, when moving toward the equator, the precipitating flux falls below and then rises above the trapped particle fluxes before the final deep decrease of the J_P/J_T ratio. Here we shall use the final drop of the J_P/J_T ratio as the definition of the IB. The scale of these small structures is typically about 0.5° invariant latitude.

2. The latitude of the IB position seems to be inversely related to particle rigidity. This is demonstrated for protons of different energies in an expanded scale at the lower panels of Figures 1 and 2.

3. Polewards of the isotropic boundary the ratio J_P/J_T remains nearly constant in spite of large variations in particle fluxes. This indicates that the degree of the loss cone filling does not depend critically on the value of particle flux inside the isotropic zone.

4. The IB of energetic protons is found in the equatorward half (in the diffuse zone) of the auroral precipitation on the nightside, and equatorwards of the intense auroral precipitation at dayside and dusk. Therefore it lies well inside of the closed field lines of the plasma sheet. On the other hand, the IB of energetic electrons on the nightside is often found in the poleward part of the auroral oval (in the structured precipitation region). The electron IB was rarely seen at dayside.

The first three characteristics (apart from the small-scale structures mentioned in point 1) are ordinary features of the nightside pattern of the energetic particle precipitation and are well documented in the past studies by *Imhof et al.* [1977, 1979], *Lundblad et al.* [1979], and *Sergeev et al.* [1983]. Our survey of more than 300 orbits in August 19–23, 1979, and November 21–30, 1981, spanning all MLT sectors, supports the common occurrence of this pattern. The good MLT coverage allows us also to comment on the MLT dependence of the IB position. The same morphology of the proton precipitation seems to hold true for all activity conditions as well as for all MLT sectors including dayside. However, there is a pronounced MLT variation of the IB latitude. Figure 3 shows the invariant latitudes of the isotropic boundaries of 80 keV protons observed over many successive orbits during two periods characterized by relatively steady solar wind and interplanetary magnetic field (IMF) parameters. The first (August 23, 1979) was a 10-hour-long quiet period with AE < 100 nT, $Kp \leq 1$, IMF B_z = 0–2 nT, IMF B_y = -2–2 nT, and $V_{sw} \simeq$ 400 km/s. As can be seen in Figure 3, the isotropic boundaries in the two hemispheres agree well with each other and form a continuous MLT pattern with a distinct noon-midnight asymmetry. During the other, more disturbed interval on August 21, 1979 (AE = 500–700 nT, Kp = 4–5, IMF $B_z \simeq$ -4 nT, IMF B_y= -1 – -3 nT, $V_{sw} \simeq$ 650 km/s) there is more scattering in data points, but the MLT dependence and the noon-midnight asymmetry are qualitatively the same. However, the latitudes of the isotropic boundaries are 3 to 5 deg lower than during the more quiet period.

2.2. *Interpretation of the Isotropic Boundary in Terms of Tail Current Sheet Scattering Mechanism*

The pitch angle distributions of particles on closed field lines may display a strong flux depletionin the loss cone due to collisions in the ionosphere. In particular, when

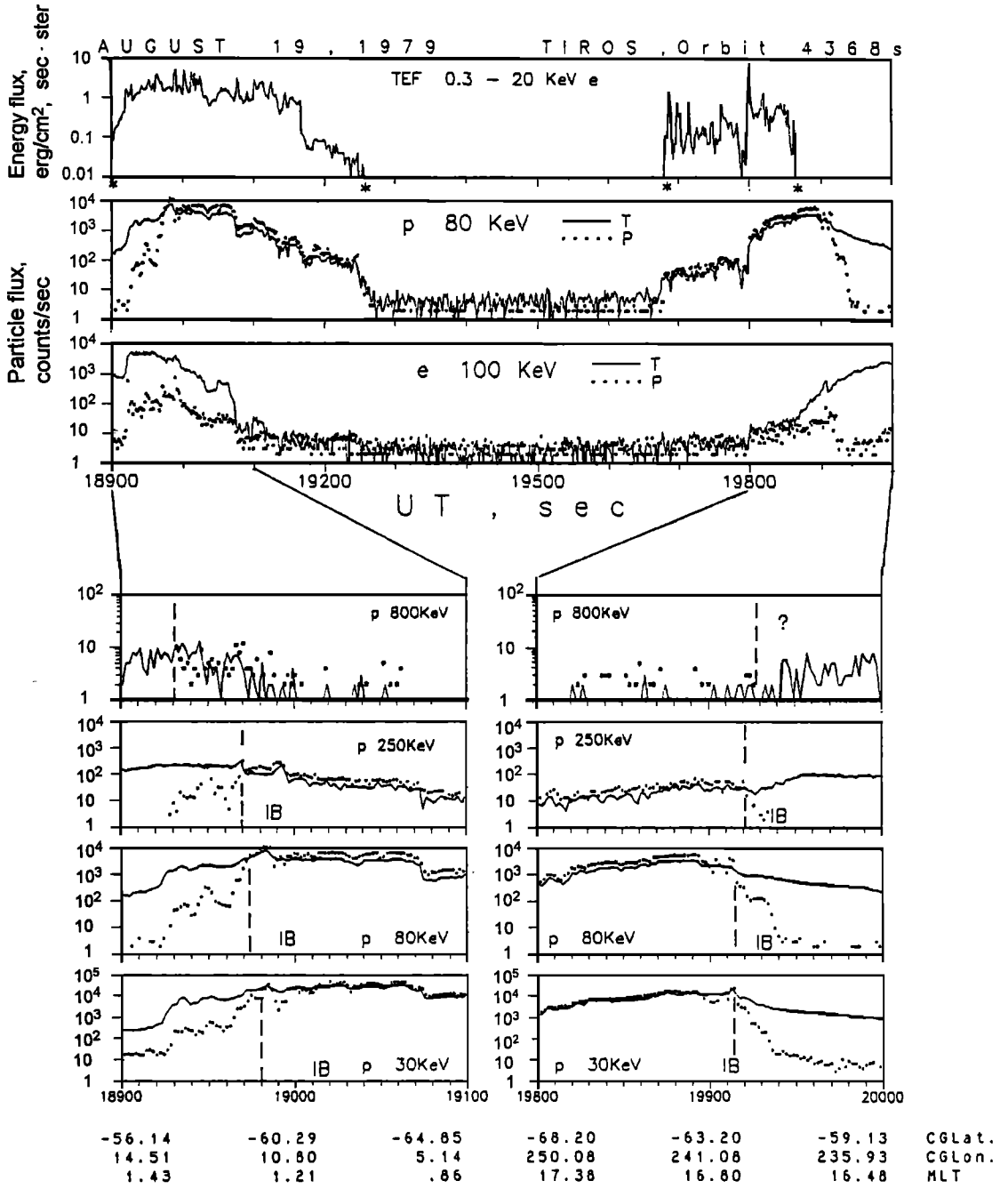

Fig. 1. Particle flux variations observed by the TIROS spacecraft in early morning to afternoon MLT sectors in the southern hemisphere during orbit 4368. Precipitating and trapped fluxes are shown by dotted and solid lines, respectively. The upper panel illustrates the auroral electron energy flux from the TED sensor. The second and third panel give the 80–250 keV proton and >100-keV electron fluxes from the MEPED sensor. The lower plots show inexpanded scale a few proton fluxes in the vicinity of their isotropic boundaries marked by vertical dashed lines.

observing the downgoing particles at low altitudes above the ionospheric loss region, the relative amount of particles inside the loss cone can be used to measure the amount of pitch angle scattering during one bounce between the opposite mirror points. In the absence of wave-particle interaction, the depleted loss cone will be conserved for adiabatically moving particles. However, possible nonadiabaticity or stochastization of particle motion will lead to the filling of the loss cone. For those particles that mirror at low altitudes (having small equatorial pitch angles), the deviations from adiabatic motion are strongest at the equator in the central current sheet. Adiabaticity is primarily controlled by the equatorial value of the ratio R_c/ρ, where R_c is the curvature radius of the field line, $\rho = mVc/eB_z = G/B_z$ is the effective particle gyroradius, V is the total particle velocity, and G is particle rigidity. According to the numerical simulations of trajectories of small pitch angle particles [*Sergeev et al.*, 1983; *Sergeev and Malkov*, 1988], the threshold condition for strong pitch angle scattering (scattering to the center of loss

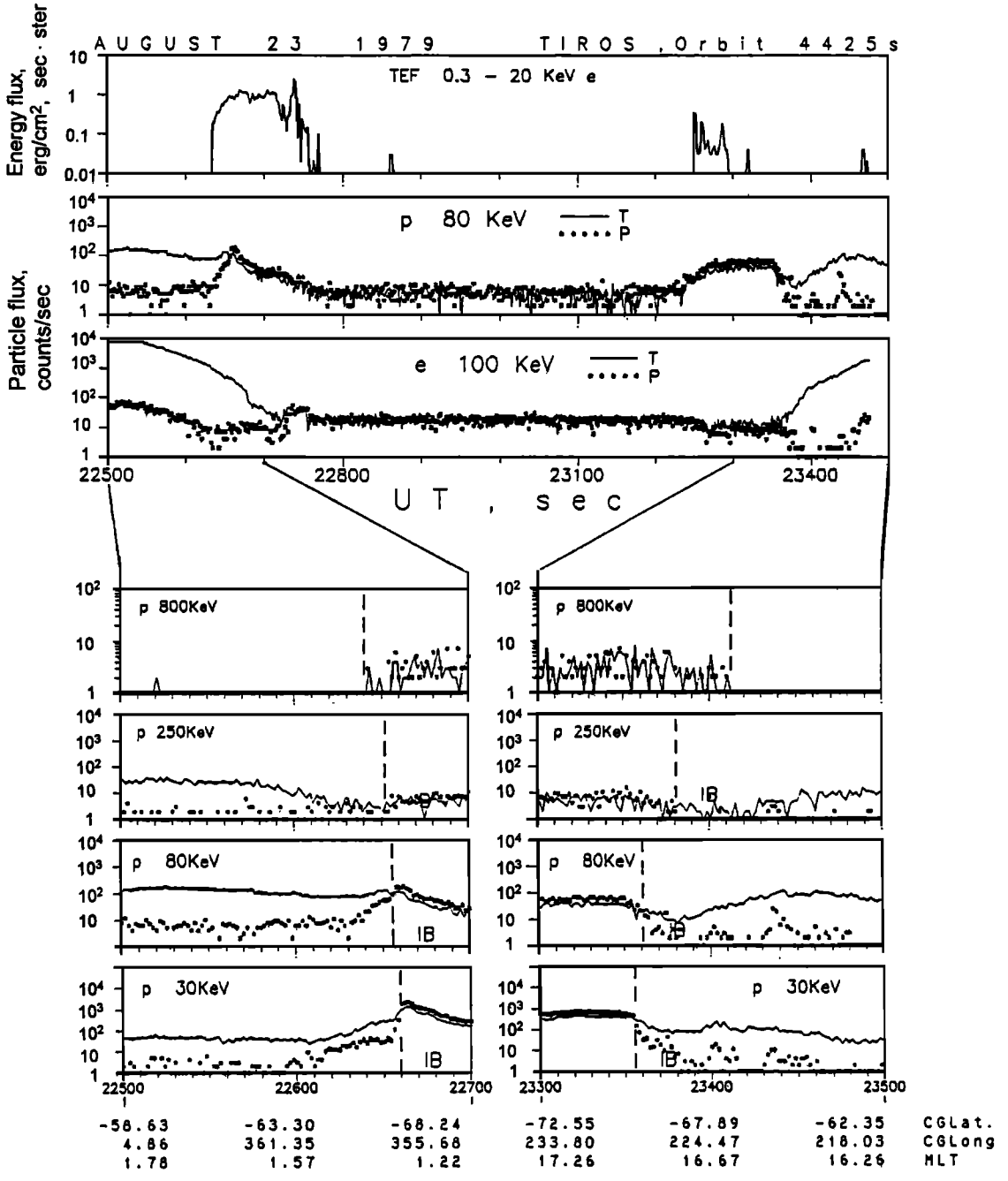

Fig. 2. Same as Figure 1 for orbit 4425.

cone) is approximately as follows:

$$R_c/\rho = B_z^2(GdB_x/dz)^{-1} \leq 8 \qquad (1)$$

where the equality sign corresponds to the isotropic boundary. As seen in equation (1), the threshold condition for isotropic precipitation includes only particle rigidity which is known from low-altitude measurements and parameters of the equatorial magnetic field with B_z appearing as the main controlling parameter.

As shown in Figure 4, due to the monotonic decrease of equatorial B_z with a distance into the tail, the closed field line region is divided in two parts. The inner part corresponds to the adiabatic case where the depleted loss cone is conserved. In the outer part the loss cone is refilled because of stochastic particle motion when crossing the equatorial current sheet. The boundary between these regions is the isotropic boundary. This simple pattern of two regions with different types of particle dynamics at the equator is always valid for protons due to the high threshold B_z value (see Figure 4*b*). Computations based on the T89 models [*Tsyganenko*, 1989] for 80 keV protons find threshold B_z values and IB positions at nightside between 40 nT at $r = 7.8$ R_E ($Kp = 0$) and 80 nT at $r = 6.3$ R_E ($Kp = 4$) and in the dawn-dusk meridian from about 20 nT to 30 nT and $r = 10$–12 R_E.

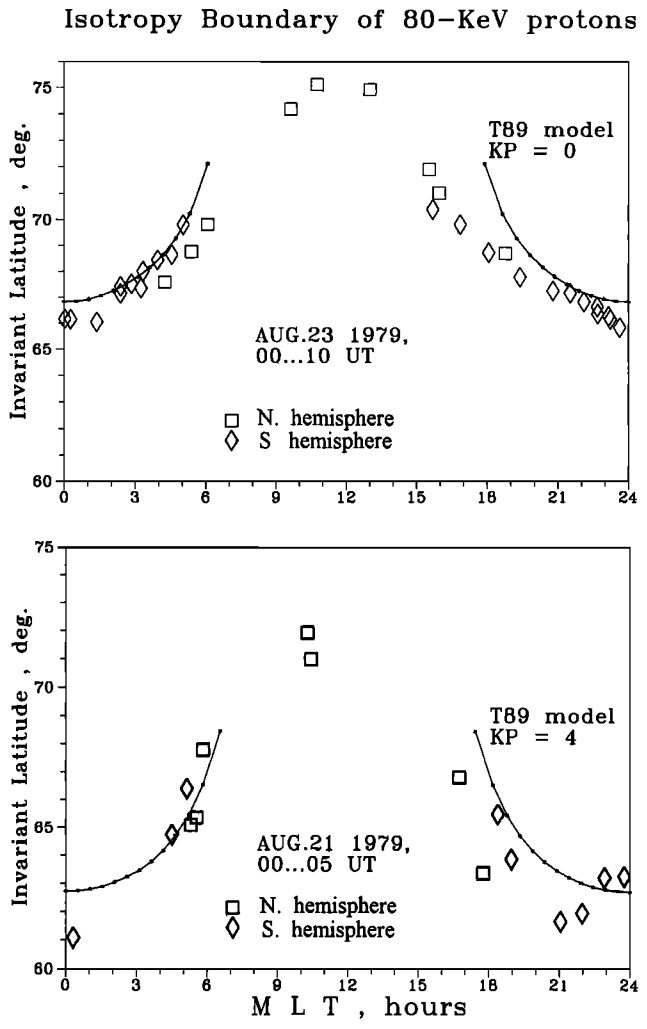

Fig. 3. Dependence of the invariant latitude of 80 keV proton isotropic boundary on magnetic local time during (top) a long quiet and (bottom) a more active period as inferred from successive passes of NOAA/TIROS and NOAA-6 spacecraft.

Because of the much lower rigidity of electrons, the corresponding threshold B_z values for electron IB are lower and the boundaries are in a magnetic field region mainly controlled by the tail current. The monotonic decrease of the radial B_z profile may not necessarily be valid in this region since the redistribution and filamentation of the tail current and other dynamic phenomena like plasmoids may generate bumps and gaps on this profile. In such a case, as schematically shown by the dashed line in Figure 4*b*, there may be a few detached isotropic precipitation regions. As a result of such possible structuredness and time variability of B_z, the pattern and latitudinal position of the isotropic boundary is expected to be more variable for electrons than for protons. Because of these differences between the electron and proton isotropic boundaries the proton is more suitable for testing the IBA algorithm. Another reason in favor of the proton is that the proton IB lies close to the geostationary orbit where magnetic measurements are regularly made.

In Figure 3 we have also plotted the MLT dependence of the IB for 80-keV protons as obtained from the T89 model for the corresponding activity level. This was done by finding that point in the equatorial magnetosphere at the respective MLT sector where equality (1) was fulfilled and then projecting this point along the model field lines intothe ionosphere. Figure 3 shows a fairly good agreement between the observed and computed isotropic boundaries within 4–5 hours of MLT around midnight. However, closer to the dusk-dawnmeridian the difference between the observed and computed IB positions increases, and about 2 hours further to noon at about 0800 and 1600 MLT the IB could not be determined by the model. This inconsistency will be discussed later in section 4.

2.3. *Basic Features of the Isotropic Boundary Algorithm*

The IBA method [*Sergeev and Malkov*, 1988] is based on the above discussed interpretation of isotropic boundaries of energetic particles in terms of the tail current sheet scattering mechanism. The method allows for the

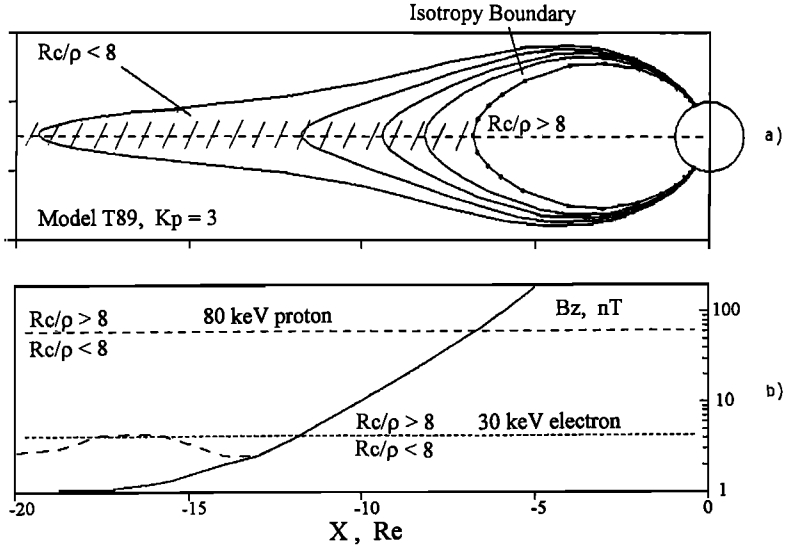

Fig. 4. (*a*) Regions of adiabatic and chaotic particle motion and the isotropic boundary as obtained from equation (1) using T89 model with Kp=3. (*b*) The radial profile of the B_z component at the equator according to the T89 (Kp=3) model (solid line). Threshold values of B_z separating the regions of adiabatic and chaotic motion of 80-keV protons and 30-keV electrons are shown as longer and shorter dashed horizontal lines, respectively. The possible inhomogeneity of B_z in the distant current-dominated plasma sheet is schematically illustrated by a dashed curve.

determination of the version of the magnetospheric model (here we use the T89 model) which leads to the best agreement between the observed and calculated position of the isotropic boundary for a given rigidity. The T89 model does not in general allow for the determination of perfect agreement since the different versions of the model are discretely ordered by the *Kp* level, and do not cover the extreme conditions in the tail. In order to overcome these shortages to some extent, the tail current of the T89 model was slightly modified by scaling it by a scalar variable *f*. Thus the original and the modified magnetic fields are as follows:

$$B_{tot}(Kp) = B_{int} + B_{res}(Kp) + B_{dr}(Kp) + B_{tail}(Kp) \quad (2a)$$

$$B_{tot}(Kp) = B_{int} + B_{res}(Kp) + B_{dr}(Kp) + f * B_{tail}(Kp) \quad (2b)$$

where B_{tot}, B_{int}, B_{res}, B_{dr}, and B_{tail} are the total magnetic field, the internal magnetic field and contributions from the magnetopause current (plus field-aligned and other currents not specified in the model), ring current and tail current system, respectively. The best fitting value of *f* was calculated for all *Kp* versions of the model. As the final outcome of this procedure we selected that *Kp* version which gave *f* closest to 1 in order not to deviate seriously from the original model. Thus, starting from input parameters including the date and time of observation, the IB coordinates (invariant latitude and MLT) and the rigidity, the IBA gives as an output the two parameters (*Kp* and *f*) specifying the best fitting magnetospheric model at the time of observations.

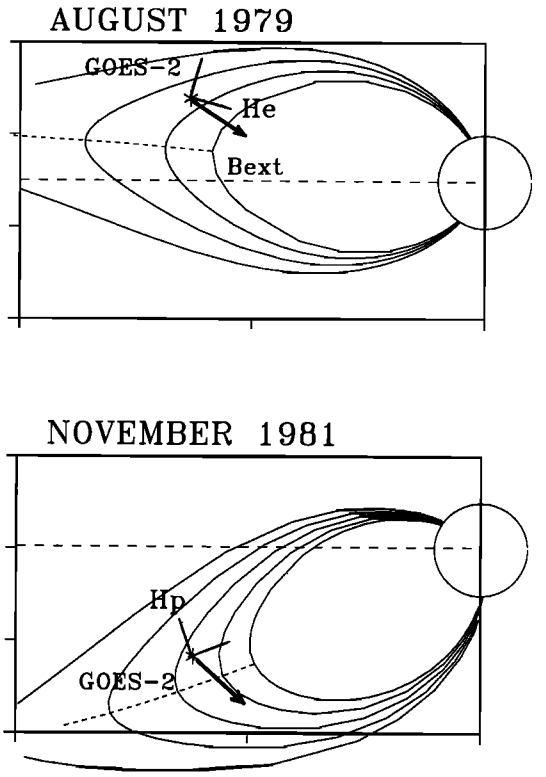

Fig. 5. Magnetic field lines of T89 (*Kp*=4) model and GOES 2 position (star) in the noon-midnight plane of GSM coordinates computed at 0700 UT for August 1979 (day 220) and November 1981 (day 320). The external magnetic field (thick arrow) is shown in the local coordinate system (HP and HE) used by GOES 2 with the preferred component indicated (HE in August and HP in November). The dashed curve indicates the central surface of the tail current sheet.

3. Comparison Of Low-Altitude and Magnetospheric Observations

3.1. *Control of the IB Position by the Tail Magnetic Field*

The low-altitude position of the isotropic boundary was compared with the tail magnetic field as simultaneously measured by the GOES 2 spacecraft during two time periods in November 21–30, 1981, and August 19–23, 1979. These intervals, which will be called below the "winter" and "summer" intervals included different activity periods with *Kp* ranging from 0 to 6.

The magnetic field measurements of the geostationary GOES 2 spacecraft (108°W; local midnight at 0712 UT) are routinely given in a local geographic coordinate system where one component is taken along the Earth rotation axis (HP), one is radial (HE; earthward positive) and one is eastward (HN). The eastward component is very small both according to observations and model and therefore it will not be included in the analysis. The main components (HP and HE) presented a different behavior and relationship with the IB positions in the two different seasons. Figure 5 visualizes the seasonal changes in geometry [see *McPherron and Barfield*, 1980] including the change of the current sheet shape and the GOES 2 position with respect to the current sheet, as well as the changes in the local coordinate system. B_{ext} indicates the magnetic field caused by external (magnetospheric) currents. Figure 5b shows that in winter the HP component varies sensitively with respect to the tail magnetic field whereas the HE component is not as sensitive. Moreover, since the spacecraft is close to the central current sheet, the HP component may even change its sign in case of vertical motions of the current sheet. In contrast, in summer the spacecraft is further away from the central current sheet and both components (HP and HE) are sensitive to the magnetic field of tail current although the HE component is slightly more influenced. Accordingly, during the two seasons different components, HP in winter and HE in summer, are better indicators of the magnetic field changes induced by the variations of tail current. Below we will refer to them as the preferred components.

Figure 6 presents our results for the comparison between low-altitude and magnetospheric observations.There we have plotted the observed IB positions of 80-keV protons versus the simultaneously measured near-equatorial tail magnetic field components. The data were only selected according to the MLT sector such that both observations were required to be within 2 hours of MLT from midnight in order to suppress the large diurnal variations (cf. Figure 3). No other selection with regard to, for example, magnetic activity, interplanetary conditions or substorm phase was applied. As seen in Figure 6, the efficient tail control of the IB position is indicated by the high correlation coefficients with the preferred magnetic components: r = 0.91 (25 data points) in November and r = -0.95 (24 points) in August. The corresponding linear regressions with the preferred components are the following:

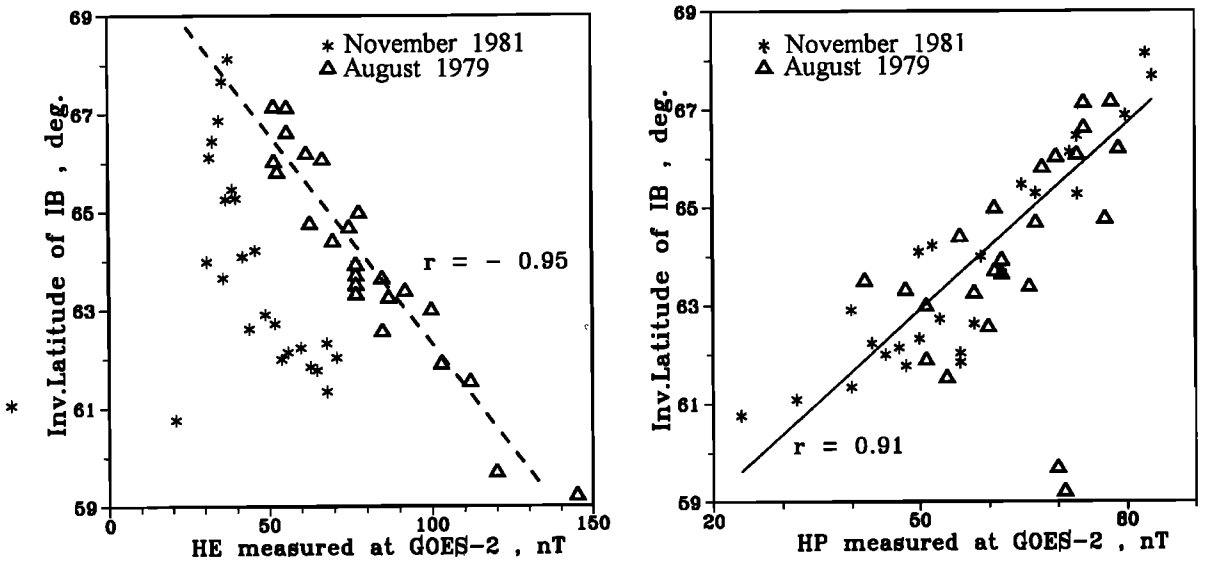

Fig. 6. The invariant latitude of the isotropic boundary of 80-keV protons compared with the two main components of the geostationary magnetic field simultaneously measured by GOES 2. Both NOAA/TIROS and GOES 2 spacecraft were required to be within 2 hours of MLT from midnight. Regression lines and correlation coefficients are given for preferred components only.

$$IB\text{Lat(deg)} = 56.6 + 0.126\ HP\text{(nT)}\ \text{(November)}\quad (3a)$$

$$IB\text{Lat(deg)} = 70.9 - 0.086\ HE\text{(nT)}\ \text{(August)}\quad (3b)$$

These relationships indicate a fairly good sensitivity of the IB position to the geostationary magnetic field since the IB invariant latitude changes by roughly 1 deg per 10 nT change in the preferred components. The standard deviations of the IB latitude in the above relations are less than 1 deg (0.86 and 0.65 deg, respectively), i.e., much less than the observed variation in the IB latitude. (As expected, the nonpreferred components show a less clear correlation and include some widely scattered data points).

3.2. *Testing the IBA Procedure*

In this section we determine the IB position for an even more extended data set by including data points from a wider MLT sector. This also allows us to test the IBA procedure outside the midnight sector. As above, we use the observed IB positions at given times as input parameters for the IBA algorithm and, using the output parameters defining the appropriate magnetospheric model, compute then the magnetic field at the location of GOES 2 using the selected model. These predicted magnetic field values are compared with the observed ones in Figure 7. We have now included all orbits where both NOAA and GOES 2 spacecraft were in the 2000–0400 MLT sector (72 data points in November and 94 in August). As seen in Figure 7 the geostationary magnetic field values predicted by the IBA procedure using low-altitude particle observations are quantitatively fairly close to the observed ones. This means that the state of the tail magnetic field is reasonably well determined by this procedure and, reversing the argument, that the observed IB positions occur very close to the field lines where the threshold condition (1) for pitch angle scattering in the current sheet is fulfilled. Again, the correlation is highest between the preferred components ($r = 0.84$ for HE component in August and 0.91 for HP component in November) and, with the exception of a few scattered data points, is also fairly good for the nonpreferred components. There is a definite pattern for data points deviating from the diagonal line of perfect correlation. Whereas for large HP and small HE values (corresponding to high IB latitude in quiet conditions; see also Figure 6) the predicted and observed magnetic fields are in nearly perfect agreement, the observed magnetic field is more depressed for small HP but more intense for large HE than the predicted magnetic field. These deviations will be discussed in more detail in section 4. The accuracy of the quantitative prediction of the geostationary magnetic field by the IBA method can be characterized by the standard deviations which were about 7 nT for the HP component in November and about 13 nT for HE in August. Since the measured value of HP (HE) varied between 20 and 100 nT (50 and 160 nT), the prediction accuracy is only about 10 % of the whole dynamic range of these magnetic components. Note that in order to achieve this accuracy in predicting the magnetic field at the geosynchronous distance, it was necessary to determine separate regression equations for each season.

As already mentioned, the above analysis was based on the isotropic boundaries of 80-keV protons. We have also tested 30 and 250 keV protons and obtained similar results. As an example of the consistency of obtained predictions, Figure 8 shows the comparison of HP components predicted by the IBA using 30- and 250-keV protons. A regular pattern of deviation is seen in Figure 8 such that the 30-keV protons, whose isotropic boundary is located further from the Earth than that of 250 keV protons, require a more depressed (by about 5 to 7 nT) and more stretched magnetic field. This indicates that the true equatorial magnetic field gradient is larger than included in the magnetic field model. We will further discuss this point in the following section.

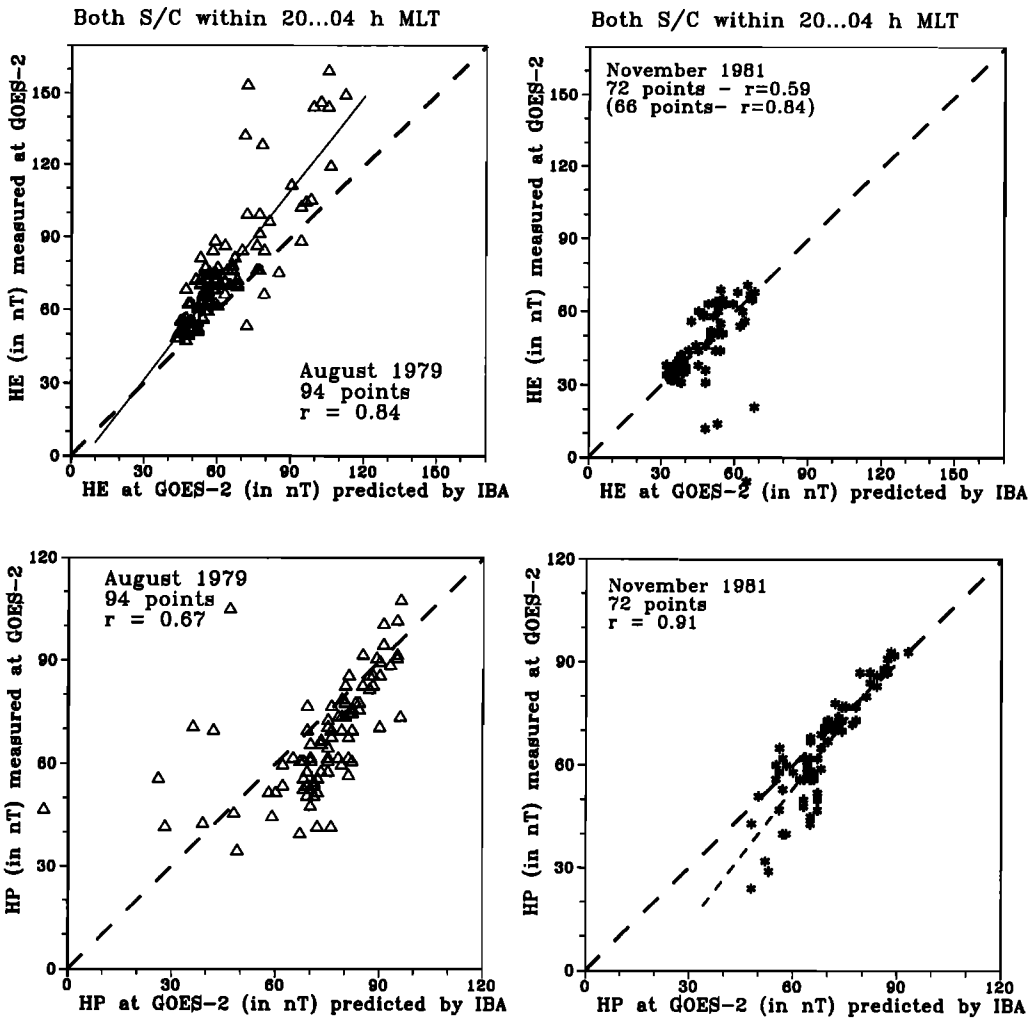

Fig. 7. The HE and HP components measured by GOES 2 compared with those predicted by the IBA method over two time periods. The NOAA/TIROS and GOES 2 spacecraft were now within the 2000–0400 MLT sector. Regression lines are shown for preferred components only.

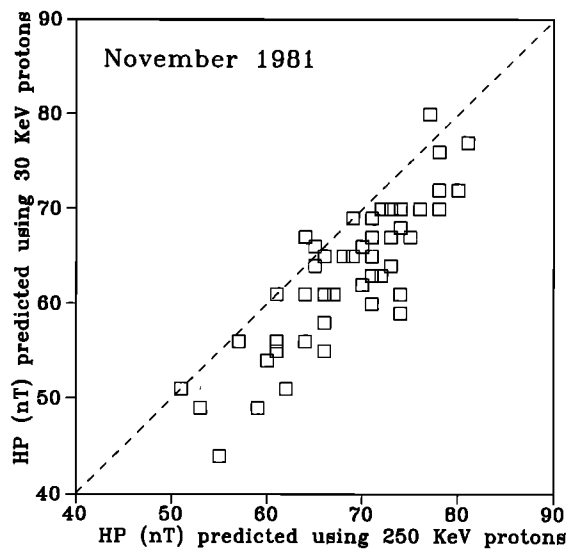

Fig. 8. Comparison between the two HP components calculated using the IBA method from the observed isotropic boundaries of 30- and 250-keV protons.

4. Discussion

4.1. *Tail Current Sheet Scattering as the Dominant Mechanism of Isotropic Precipitation*

Wave particle interactions were long considered to be the main mechanism leading to pitch angle scattering of magnetospheric particles, and the measured particle precipitations were interpreted entirely in terms of this mechanism (see, for example, a review by *Hultqvist*, [1979]). Although the principle of pitch angle scattering in magnetic field regions where the conditions for adiabatic particle motion are violated was known since the early age of magnetospheric physics [see *Alfvén and Fälthammar*, 1963], this mechanism has so far been applied, for example, to solar protons but not to auroral or energetic magnetospheric particles. On the other hand, during recent years the theoretical importance of chaotic (nonadiabatic) effects for the tail plasma sheet has been widely recognized [see *Büchner and Zelenyi*, 1987] (also see papers in the special issue of *Geophysical Research Letters, 18* (8), 1991).

There are many uncertainties in explaining the isotropic precipitation of energetic particlesin terms of the wave particle interaction mechanism. First, there is no

sufficiently detailed picture of wave characteristics over the vast plasma sheet region where isotropic precipitation is observed. (We would like to remind the reader that the region of isotropic proton precipitation extends from the geosynchronous orbit up to the outer boundary of plasma sheet; see Figures 1 and 2.) Second, even in cases when there is experimental information about waves, it is often not straightforward to decide whether they are able to produce the strong diffusion required to fill the loss cone isotropically. Also, the wave intensity is in general structured and depends on the activity and certainly on particle fluxes, in sharp contrast to the observed properties of the isotropic precipitation of energetic particles.

On the other hand, the properties of the TCS mechanism are in agreement with all observational facts. These include the formation of a broad zone of isotropic precipitation on closed field lines of plasma sheet with a sharp equatorward boundary. Moreover, the fact that the strong pitch angle scattering inside this zone does not depend on particle fluxes or activity conditions, and the rigidity dependence of the isotropic boundary can naturally be explained by the TCS mechanism.

As shown in section 3, the equatorial magnetic field required to produce the isotropic boundary at its observed position generally agrees with the observed magnetic field. The systematic deviations of the predicted and observed magnetic field values (see Figure 7) give evidence for an even more stretched magnetic field than required for strong scattering. Similar results were earlier obtained from the in situ observations of particle pitch angle distributions and equatorial magnetic field by the OGO 5 spacecraft [*West et al.*, 1978]. This proves that TCS mechanism is acting on the IB field lines and consequently on the more tailward field lines also. Moreover, intense particle scattering produced by the TCS mechanism on the stretched field lines may suppress possible microinstabilities by suppressing the pitch angle anisotropy required for their excitation. In agreement with these and other earlier findings [e.g., *Sergeev et al.*, 1983], we may state that the TCS mechanism is evidently the dominant mechanism leading to the isotropic precipitation of energetic protons.

4.2. *IBA as a Predictor of the Instantaneous Magnetic Field*

It is well known that the Kp index (or any other magnetic index) does not describe the magnetic configuration reliably [*Fairfield*, 1991; *Malkov and Sergeev*, 1991]. To see this, we have plotted in Figure 9 the Kp number of the magnetospheric model as determined from the IBA procedure against the actual Kp value at the time of IB measurement. A weak overall correlation can be seen but the data points are widely spread. For example, when the real Kp is 2 or 3, many events require a magnetospheric configuration corresponding to model version of Kp = 5. Similarly, a large variation in the observed magnetic configuration (especially lobe field strength and amount of tailward stretching) was demonstrated by *West et al.* [1978] for quiet conditions (Kp = 0–1).

In Figures 6 and 7 we saw some widely scattered data points. Most of them were found in conditions of highly disturbed solar wind when the solar wind velocity may briefly deviate from radial direction by up to 10–15 deg. Then the neutral sheet surface may be inclined

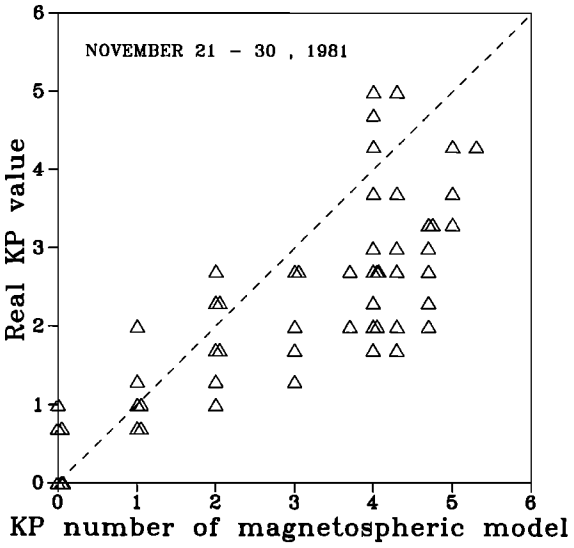

Fig. 9. The Kp index of the magnetospheric model obtained from the IBA procedure versus the simultaneous value of the real Kp index.

by up to 1 R_E from its nominal position even at the geosynchronous distance, and the comparison with the model predictions is meaningless. Therefore, although no high time resolution solar wind data were available to verify this, we believe that the inconsistent data points in Figures 6 and 7 reflect the need to take into account the effects of nonradial solar wind flow when interpreting the geostationary magnetic field observations.

The results of Figure 7 showed a surprisingly good correlation between the predicted and observed magnetic field although we did not select the data according to activity level or substorm phase, and although the low-altitude and magnetospheric spacecraft could be separated by up to 8 hours of MLT. This shows that the magnetic field in the near-Earth magnetotail is mostly influenced by large-scale current systems rather than relatively localized current systems. (A detailed investigation of the substorm phase effects is retained for later work.) The relatively small standard deviation between the predicted and observed magnetic fields, which was only about 10 % of the total dynamical range, makes it possible to use low-altitude energetic particle observations in monitoring the tail magnetic field as well as in magnetic field mapping. The accuracy of the method can still be increased, for example, by using the isotropic boundaries of particles with different energies. This idea was tested in the paper by *Sergeev and Malkov* [1988] but was not used here because of the insufficient energy resolution of the SEM instruments on board NOAA spacecraft.

4.3. *Inconsistencies of the Magnetospheric Models Implied by the IBA Analysis*

Earlier comparisons of the observed IB latitude and rigidity profiles with those computed from magnetospheric models [*Popielawska and Zwolakowska*, 1991; *Imhof*, 1988] implied a more depressed and stretched magnetic field in the near-Earth region, i.e., larger radial gradients in the equatorial magnetic field than given by the model. These studies used earlier Tsyganenko models which include a smaller depression and tailward stretching than the latest

Tsyganenko model (T89) used in our analysis. However, even using the T89 model, Figure 7 indicates that during the most active conditions (most depressed field) the observed HP component is up to 20 nT weaker than the predicted one. Also, the systematic deviations in Figure 8 using different proton energies imply larger field gradients in the near-Earth region. This interpretation is further supported by comparisons between the observed and model magnetic fields made by *Tsyganenko* [1990], *Fairfield* [1991], and *Malkov and Sergeev* [1991]. Concluding, the systematic deviations observed in Figures 7 and 8 are mainly associated with the shortcomings of the applied magnetic field model.

Let us now turn back to the MLT dependence of the isotropic boundary shown in Figure 3. We did not find any difference in the isotropic boundary or precipitation characteristics of protons between dayside and nightside. Furthermore, no discontinuity was found to exist between these two regions. As discussed above and seen in Figure 3, the model computations did not fulfill the threshold condition of equation (1) in the dayside magnetosphere. Instead, those parts of the modeled isotropic boundary that are closest to noon are really on field lines threading toward the expected position of the low-latitude boundary layer, i.e., toward the flanks of the magnetopause. The observed inconsistency between observations and computations can be understood if the dayside field lines emanating from the dayside cleft region are actually more tailward stretched than given by the model. This agrees with the recent results by P.L. Izraelevitch and N.S. Nikolaeva (preprint, 1991) who compared the same model field (T89) with the observational data used originally by *Tsyganenko* [1989] for constructing this model. Computing the differences between the observed and modeled magnetic field and averaging these differences along individual flux tubes they found large systematic deviations of more than 50 % in the tubes emanating from the wide region around the nominal dayside cleft location. They concluded that the T89 model seriously underestimates the tailward stretching of these field lines. Therefore we believe that most of the remaining inconsistencies between the modeled and observed properties of the proton isotropic boundary result from the defaults of the imperfect magnetic field model rather than from the IBA method itself. Moreover, we are confident that the isotropic boundary method can be used as a tool to check the consistency of future magnetic field models.

5. Conclusions

In this paper we have studied the equatorial boundary of the isotropic precipitation of energetic (>30 keV) protons (in brief isotropic boundary, IB) measured by the low-altitude NOAA spacecraft. We compared the invariant latitude and MLT shape of the observed IB with model predictions based on the T89 magnetospheric model and the threshold condition of particle scattering in the current sheet. We also calculated the nightside equatorial magnetic field using the model selected by the isotropic boundary algorithm (IBA) and compared it with the field measured simultaneously by GOES 2 spacecraft. The results ofour study can be summarized as follows:

1. The observed IB invariant latitude and its variation with MLT at nightside agree fairly well with the values predicted by the T89 model. However, there are considerable deviations at the dayside.

2. The IB latitudes on the nightside are strongly controlled by the tail equatorial magnetic field. We found a correlation coefficient larger than 0.9 when comparing data from the two regions without selecting it according to, for example, magnetic activity or any other way. The best correlation was found for preferred field components which, depending on the seasonal changes, experience the largest influence of the tail current sheet.

3. The preferred magnetic field components predicted by the IBA method display a high correlation with the corresponding field components measured by GOES 2. The standard deviation of this correlation was only about 10 % of the dynamic range of these components. This demonstrates the great predictive capability of the IBA method in monitoring the magnetic field in the near-Earth tail.

4. All above mentioned results (the strong control of the IB position by the tail magnetic field, the correlation of the observed and predicted values of the equatorial magnetic field, and the MLT variation and the rigidity dependence of the IB latitude) strongly support the view that particle scattering in the equatorial current sheet (tail current sheet scattering) is, at least on the nightside, the dominant mechanism producing the isotropic precipitation of energetic protons.

5. Systematic differences between the predicted and observed IB latitudes at dayside were found. Furthermore, indirect evidence was obtained for a more tailward stretched magnetic field at the geosynchronous orbit on the nightside. These are interpreted as being due to systematic inconsistencies of the T89 magnetospheric field which was used in the IBA procedure.

Summarizing, the low-altitude observations of isotropic boundaries of energetic particles can be used as a powerful tool to obtain information on the instantaneous magnetic field configuration and to test the global structure of present and future magnetospheric models.

Acknowledgments. The particle observations from NOAA and GOES spacecraft were made available to us through the WDC-A for STP in Boulder. We thank N. A. Tsyganenko for valuable discussions and T. Bösinger and T. Bräysy for their assistance in this work. The authors were supported by the Russian Finnish Working Group on Geophysics. K.M. also acknowledges the support of the Academy of Finland.

The Editor thanks D.H. Fairfield and W.L. Imhof for their assistance in evaluating this manuscript.

References

Alfvén, H., and C. G. Fälthammar, *Cosmic Electrodynamics, Fundamental Principles*, 2nd ed., Clarendon, Oxford, 1963.

Büchner, J., and L. M. Zelenyi, Chaotization of the electron motion as the cause of an internal magnetotail instabilityand substorm onset, *J. Geophys. Res., 92*, 13,456, 1987.

Fairfield, D. H., An evaluation of the Tsyganenko magnetic field model, *J. Geophys. Res., 96*, 1481, 1991.

Hill, V. J., D. S. Evans, and H. H. Sauer, TIROS/NOAA satellites Space Environment Monitor, Archive tape documentation, *NOAA Tech. Mem. ERL SEL-71*, 50 pp., Environ. Res. Lab., Boulder, Colo., 1985.

Hultqvist, B., The hot ion component of the magnetospheric plasma and some relations to the electron component – Observations and physical implications, *Space Sci. Rev., 23*, 581, 1979.

Imhof, W. L., Fine resolution measurements of the *L*-dependent energy threshold for isotropy at the trapping boundary, *J. Geophys. Res., 93*, 9743, 1988.

Imhof, W. L., J. B. Reagan, and E. E. Gaines, Fine-scale spatial structure in the pitch angle distributions of energetic particles near the midnight trapping boundary, *J. Geophys. Res., 82*, 5215, 1977.

Imhof, W. L., J. B. Reagan, and E. E. Gaines, Studies of the sharply defined *L* dependent energy threshold for isotropy at the midnight trapping boundary, *J. Geophys. Res., 84*, 6371, 1979.

Lundblad, J. A., F. Søraas, and K. Aarsnes, Substorm morphology of > 100 keV protons, *Planet. Space Sci., 27*, 841, 1979.

Malkov, M. V., and V. A. Sergeev, Characteristic anomalies of the magnetospheric configuration under stable convection activity, *Geomagn. Aeron., 31*, 578, 1991.

McPherron, R. L., and J. N. Barfield, A seasonal change in the effect of field-aligned currents atsynchronous orbit, *J. Geophys. Res., 85*, 6743, 1980.

Popielawska, B., and D. Zwolakowska, An assessment of a magnetospheric model by tracing the energetic particle trapping boundary, *Geophys. Res. Lett., 18*, 1489, 1991.

Pulkkinen, T. I., D. N. Baker, D. H. Fairfield, R. J. Pellinen, J. S. Murphree, R. D. Elphinstone, R. L. McPherron, J. F. Fennell, and R. E. Lopez, Modeling the growth phase of a substorm using the Tsyganenko model and multi-spacecraft observations: CDAW-9, *Geophys. Res. Lett., 18*, 1963, 1991.

Pulkkinen, T. I., D. N. Baker,R. J. Pellinen, J. Büchner, H. E. J. Koskinen, R. E. Lopez, R. L. Dyson, and L. A. Frank, Particle scattering and current sheet stability in the geomagnetic tail during the substorm growth phase, *J. Geophys. Res., 97*, 19,283, 1992.

Sergeev, V. A., and M. V. Malkov, Diagnostics of the magnetic configurationof the plasma layer from measurements of energetic electrons above the ionosphere, *Geomagn. Aeron., 28*, 549, 1988.

Sergeev, V. A., E. M. Sazhina, N. A. Tsyganenko, J. A. Lundblad, and F. Søraas, Pitch angle scattering of energetic protons in the magnetotail current sheet as the dominant source of their isotropic precipitation into the nightside ionosphere,*Planet. Space Sci., 31*, 1147, 1983.

Sergeev, V. A., P. Tanskanen, K. Mursula, A. Korth, and R. C. Elphic, Current sheet thickness inthe near-Earth plasma sheet during substorm growthphase, *J. Geophys. Res., 95*, 3819, 1990.

Siscoe, G. L., What determines thesize of the auroral oval?, in *Auroral Physics*, ed., C.-I. Meng, M. J. Rycroft, and L. A. Frank, p. 159, Cambridge University Press, New York, 1991.

Tsyganenko, N. A., A magnetospheric magnetic field model with a warped tail current sheet, *Planet. Space Sci., 37*, 5, 1989.

Tsyganenko, N. A., Quantitative models of the magnetospheric magnetic field: Methods and results, *Space Sci. Rev., 54*, 75, 1990.

West, H. I., R. M. Buck, and M. G. Kivelson, On the configuration of the magnetotail near midnight during quiet and weakly disturbed periods: Magnetic field modelling, *J. Geophys. Res., 83*, 3819, 1978.

M. Markov, Polar Geophysical Institute, 184200 Apatity, Russia.

K. Mursula, Department of Physics, University of Oulu, SF-90570 Oulu, Finland.

V. A. Sergeev, Institute of Physics, University of St. Petersburg, 198904 St. Petersburg, Russia.

(Received July 10, 1992;
revised October 5, 1992;
accepted October 28, 1992.)